Study of Explosive and Nonexplosive Cyclogenesis during FGGE

CARLYLE H. WASH, ROBERT A. HALE, PAUL H. DOBOS, AND ERIC J. WRIGHT

Department of Meteorology, Naval Postgraduate School, Monterey, California

(Manuscript received 30 November 1990, in final form 10 June 1991)

ABSTRACT

Explosive cyclogenesis during the winter of the First Global GARP Experiment (January–February 1979) is analyzed using the revised European Centre for Medium Range Weather Forecasts (ECMWF) analyses. Explosive cyclogenesis is defined as a decrease in the sea level pressure at the rate of 1 mb h^{-1} for at least 12 h. Diagnostics for 23 explosively developing cases and 16 nonexplosive cases are evaluated. Parameters compared include the dry static stability, low-level relative vorticity, vorticity advection, upper-level divergence, kinematic vertical velocities, and the strength of the low-level baroclinity. These parameters are compared statistically at the initial, 12-, and 24-h time periods. Parameters for which the explosive and nonexplosive cyclone ensembles were statistically separable are the kinematic vertical velocity and the upper-level divergence and vorticity advection. The strong upper-level processes for the explosive cases at the initial time indicate the importance of upper-tropospheric features in producing the stronger vertical motions and more rapid cyclogenesis.

1. Introduction

During the past decade a major focus of extratropical cyclone research has been to understand explosive oceanic development. A catalyst for this activity was the synoptic–dynamic climatology of these systems by Sanders and Gyakum (1980). Additional climatological studies of rapid cyclogenesis by Roebber (1984) and Gyakum et al. (1989) have provided better descriptions of the location and frequency of occurrence of these systems. In addition, many cyclone case studies and model simulations have been completed describing upper- and lower-tropospheric processes important in rapid development.

Several recent studies have composited data from many storms or studied a collection of storms to generalize results from the various case studies. Rogers and Bosart (1986) composited ocean weather ship rawinsonde data from the North Atlantic and Pacific oceans for a 10-year period to study the thermodynamic structure for different stages of rapid development. Their results from 328 cases showed that oceanic rapid deepeners develop initially in strongly baroclinic low-level environments, with the cyclones evolving into deep and intense vortices characterized by strong baroclinicity, strong low- and midlevel ascent, and evidence of low-level conditional instability. Since the compositing of the rawinsonde data was done relative to the developing surface centers, the inherent smoothing in the compositing process makes study of the details of the mid- and upper-level features difficult.

Sanders (1986) composited surface pressure centers and studied the associated 500-mb absolute vorticity maxima for 48 cases of explosive cyclogenesis over the west-central North Atlantic Ocean. Sanders found that a 500-mb vorticity maximum, located upstream, preexisted the surface cyclone in all cases, and a high correlation was found between 500-mb cyclonic vorticity advection over the surface cyclone and simultaneous surface deepening rate.

Recently Manobianco (1989) constructed composites of 24 of the 48 Sanders cases using daily European Centre for Medium Range Weather Forecasts (ECMWF) analyses. The three-dimensional structure of the composited fields described the mean structure of rapidly developing systems, including the presence of an upper-tropospheric disturbance; however, specific cyclogenesis features such as the development of a tropopause fold or a well-defined upper-level jet streak were not resolved.

Ensembles of numerical forecasts have also been studied to identify the key factors in forecasting explosive cyclone development. Kuo and Low-Nam (1989) used the Penn State–NCAR mesoscale model to study nine rapid cyclogenesis cases, while Mullen and Baumhefner (1988) explored 11 cyclones that developed in a climate simulation run of the NCAR Community Climate Model. Both of these studies emphasized the importance of the initial conditions in forecasting these events.

This study is also directed toward generalizing the variety of case study results to gain a better understanding of rapid cyclogenesis. Rather than compos-

Corresponding author address: Prof. Carlyle H. Wash, Department of Meteorology, Naval Postgraduate School, Monterey, CA 93943-5100.

iting data or fields of data for different cases, specific diagnostic terms are evaluated for a collection of 23 rapid deepening cyclone cases. Also, a collection of 16 nonrapid developers is studied for comparison. Our choice of analyses is the ECMWF final analyses for the first special observing period of the First Global GARP Experiment (FGGE). Instructive oceanic case studies from an earlier version of the ECMWF FGGE analyses have been completed by Wash et al. (1988). To provide a consistent framework for the cyclone diagnostics, a quasi-Lagrangian (storm-following) budget volume is used to evaluate diagnostic terms for the rapid and nonrapid deepening cyclone events. Additional details on the final ECMWF analyses are presented in the next section, followed by a description of explosive and nonexplosive storm groups. Then the diagnostic terms evaluated are described, followed by the statistical comparison of the terms from the two cyclone groups.

2. Assimilation and analyses

The scarcity of data over open-ocean areas limits the study of maritime rapid cyclogenesis. The FGGE data represented the first time a truly global dataset had been prepared (Halem et al. 1982). The sources for the FGGE data collection included surface (sea, land, and drifting buoy) reports and rawinsondes. Additional data were provided from dropsondes, aircraft, pilot balloons, and satellite measurements. The requirement for 500-km horizontal resolution was fulfilled by more than 7000 polar-orbiter satellite temperature-sounding profiles per day and 6000 cloud-drift winds from five geostationary satellites (Halem et al. 1982).

The European Centre for Medium Range Weather Forecasts (ECMWF) originally prepared 12-h analyses of the FGGE dataset for the entire year. During the special observing periods (SOPs), the analyses were completed every 6 h for 12 levels in the vertical and with a horizontal resolution of 1.875° latitude/longitude. The dataset contained both basic analysis parameters and derived ones. The original analyses were not initialized and were comprised of geopotential height, sea level pressure, and horizontal wind components. The derived terms included temperature, relative humidity, and vertical velocity at each vertical level (Bengtssen et al. 1982).

A revised ECMWF analysis was completed in 1986 (Paegle 1986). A primary difference between the main and revised dataset is the addition of worldwide synoptic and ship data, which more than doubled the original amount of data. The final dataset also included additional aircraft reports, data from three monsoon experiments, the United States special effort satellite temperatures (SATEMs) and cloud-drift winds (SATOBs), a new set of SATOB winds produced by the University of Wisconsin from Japanese GMS and Meteosat imagery and reprocessed dropsonde data (Uppala 1986).

The initial data assimilation used to produce the analyses consisted of a multivariate optimum interpolation analysis, a nonlinear normal-mode initialization, and a high-resolution model that provided a first-guess forecast. The new ECMWF assimilation used for the reanalysis of the FGGE data consisted of the following changes (Shaw et al. 1987):

- diabatic nonlinear normal-mode initialization,
- incorporation of a diurnal cycle and improved humidity analysis,
- greater vertical resolution in the upper levels,
- revision of the optimum interpolation (OI) statistics package, and
- a revision of the quality control criteria.

The ECMWF spectral model with rhomboidal truncation (T63) and mean orography was used for the revised FGGE analyses. Another improvement in the new FGGE analyses was to increase the vertical resolution from 12 to 19 levels (the horizontal resolution remained at 1.875°). The ECMWF model's physical parameterizations included a formulation of deep and shallow convection, as well as cloud and radiation schemes. Two previous weaknesses in the OI technique were unrealistically low analysis errors in data-rich areas and a high growth rate of forecast error for most regions. The solution to this problem has been to assume the revised growth rate is linear, which has resulted in better agreement with statistical estimates. In addition, the new first-guess estimates are lower and similar to upper-level geopotential values.

The updated quality control methods have introduced checks to eliminate incorrect data inputs. Shaw et al. (1987) have described certain observational platforms that have consistently provided erroneous data. These platforms have been excluded in the new analyses. The comparisons of the initial and final datasets have shown changes up to 10 mb in the Southern Hemisphere and 4 mb in the Northern Hemisphere oceans for a typical mean sea level pressure pattern (Uppala 1986). Evaluations of ECMWF analyses have shown that greater weighting has been given to the more accurate data (e.g., rawinsondes and aircraft data) when available. In data-sparse regions, such as across the open ocean, greater use of satellite data has occurred.

Substantial enhancements in the FGGE level IIIb dataset and the improved 4D data assimilation system of the ECMWF are believed to have resulted in an appreciably higher quality analysis. The locations of rapid cyclogenesis events and the calculations of the storm environment parameters rely heavily on the accuracy of this dataset.

3. Selection of explosive and nonexplosive cyclones

The region of case selection was based on the explosive cyclone climatology of the North Atlantic and Pa-

cific oceans (Sanders and Gyakum 1980; Roebber 1984). This area extended from 20° to 70°N and 170°W to 120°E for the North Pacific Ocean, and from 20° to 70°N and 0° to 85°W for the North Atlantic Ocean. The period of the evaluation was from 1 January to 28 February 1979, a portion of the first special observing period (SOP) of FGGE.

The initial screening of the storms was accomplished by Smith (1986) from sea level pressure analyses produced by the National Meteorological Center. Resulting groups of storms were revised based on the new ECMWF surface analyses. All developing cyclones over the western oceans area were considered. Since the quasi-Lagrangian budget approach was planned, all secondary cyclogenesis cases were eliminated since the diagnostic domain may include the older primary cyclone with the incipient secondary low. Any cyclone that deepened less than 5 mb in 12 h was also eliminated to exclude very weak cases. The requirement for an explosive cyclone was a deepening rate of at least 1 mb h^{-1} for a time period of at least 12 h, adjusted for latitude by the correction factor $\sin\phi/\sin 60°$ (ϕ was taken at the latitude point of the most rapid deepening). Cyclones that deepened at a lesser rate [but 5 mb $(12\ h)^{-1}$ or greater] were classified as nonexplosive. The initial time for the diagnostic study was the start of the 5 mb $(12\ h)^{-1}$ or greater development period. The diagnostics were applied to the initial time to examine factors correlated to the subsequent deepening rate of the two groups and to the next 12 and 24 h to confirm the magnitude of the resultant development. Six of the explosive cases experienced only 12 h of rapid deepening, so their statistics are included only on the 0- and 12-h times.

The center of a closed isobar (4-mb contour interval) was used to begin the initial development stage. This was true in all nonexplosive cases. In few explosive cases, explosive development occurred so rapidly that the 0-h time did not show a closed isobar. In those cases, ridging in the 500–1000-mb thickness pattern and the general structure of the surrounding isobars were used to locate the center of the budget domain. Since our primary focus is the initial development and we desired to include as many cases as possible, these events were included in the study.

The storm tracks in the North Atlantic and Pacific oceans are displayed in Figs. 1 and 2. As previously mentioned, favorable areas of explosive and nonexplosive cyclone generation are located near the western ocean boundary currents. In the North Pacific Ocean, most of the explosive storms are located east of the Japanese islands. In the North Atlantic Ocean, the storm tracks are more dominant off the east coast of the United States. Listings of the explosive Atlantic and Pacific storms (A or P) and nonexplosive cyclones (NA or NP) in the North Atlantic and Pacific oceans, as well as their 0-, 12-, and 24-h positions, are provided in Tables A1 and A2 in the Appendix. Central pressures for the 12- and 24-h periods are listed in Tables A3 and A4.

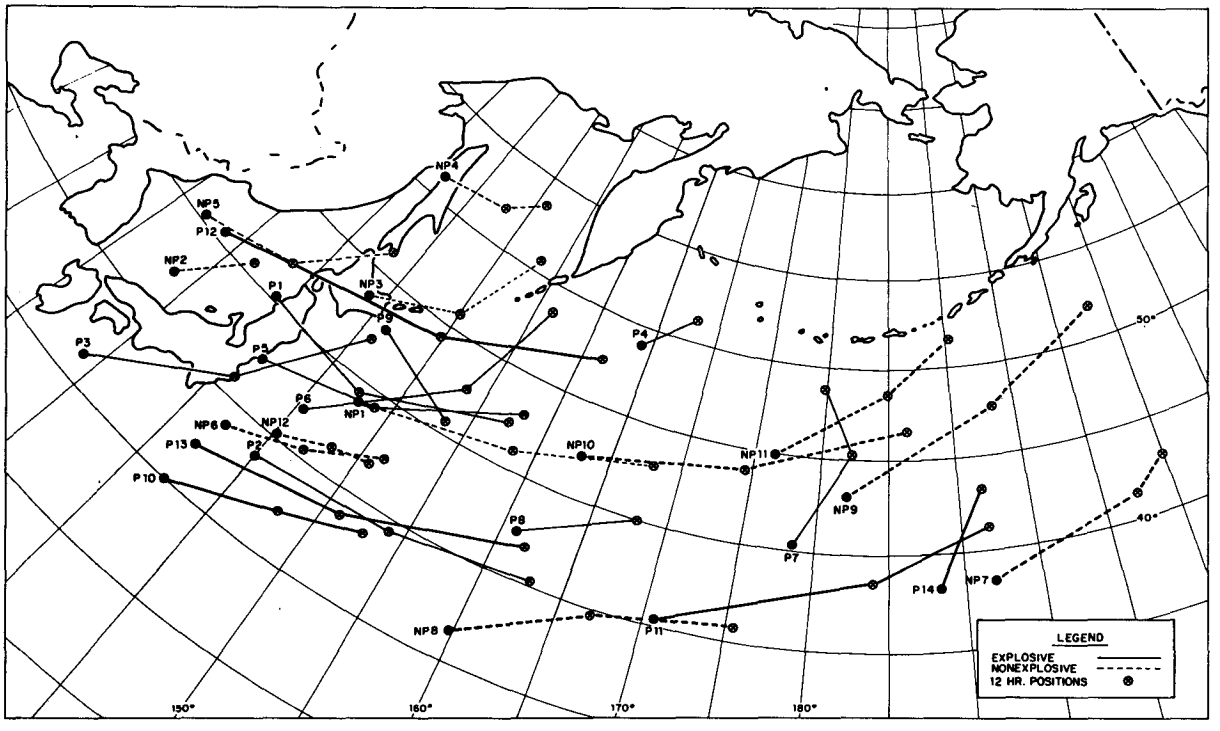

FIG. 1. North Pacific Ocean storm tracks for rapid and nonrapid deepening cyclones.

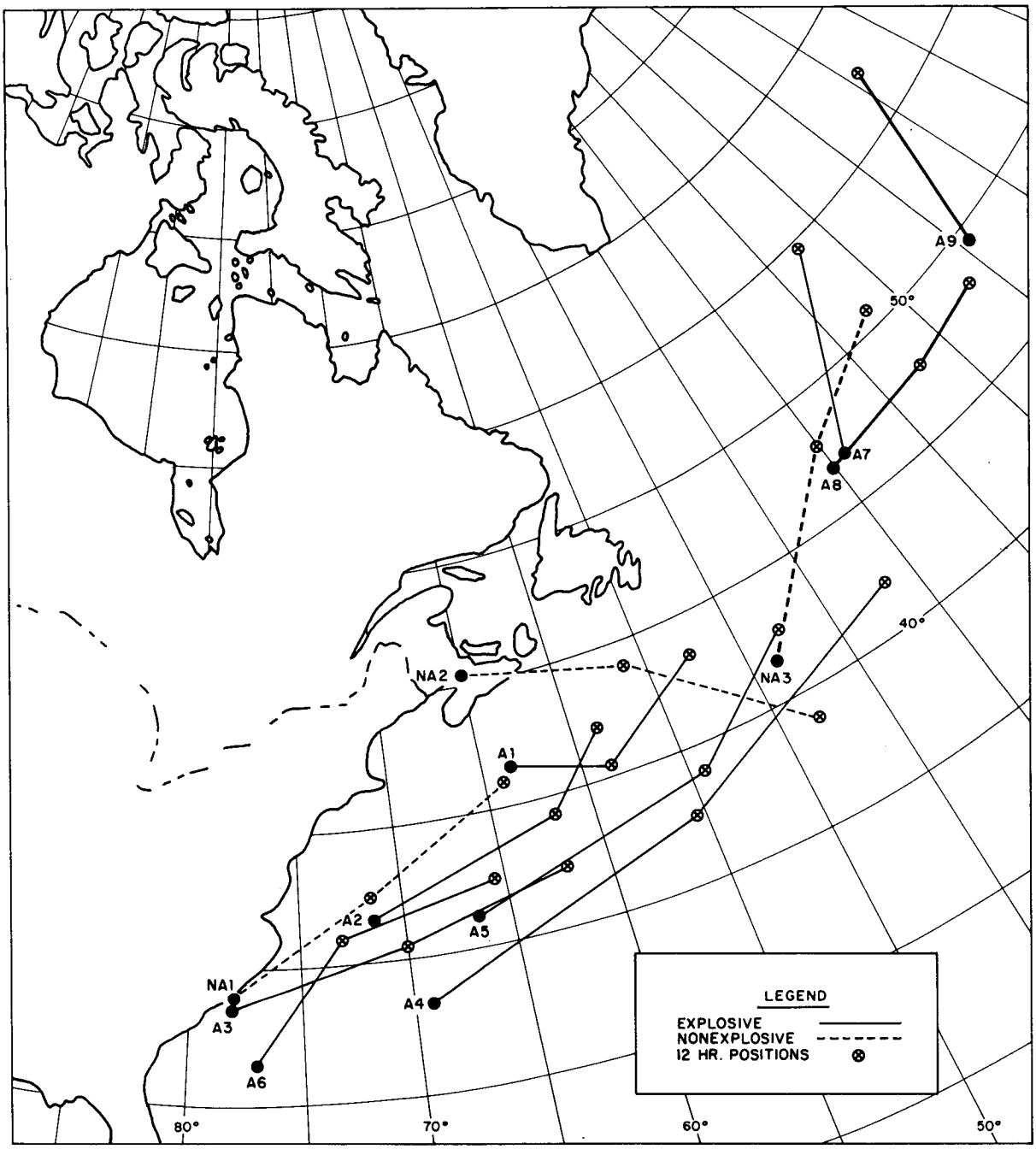

FIG. 2. North Atlantic Ocean storm tracks for rapid and nonrapid deepening cyclones.

4. Diagnostic approach

The quasi-Lagrangian diagnostic technique (Wash et al. 1988; Johnson and Downey 1975a,b) is used to evaluate cyclone development for these groups of explosive and nonexplosive storms. The primary objective of the storm-following method is to analyze cyclone development within the westerly wave regimes of the midlatitudes. The computations are performed in a spherical coordinate system that translates with the storm. The volume of the environment is centered on the lowest sea level pressure from the surface analysis. The radius of the volume around the storm is separated into 1° latitude increments. This configuration is essentially a cylindrical volume since the radius of the earth is much larger than the depth of the atmosphere.

Using this framework allows us to evaluate a number of diagnostic terms for the similar areas and quadrants of a number of storms.

Several types of cyclone development terms are reported. First, basic measures of development, changes in central and areal average SLP (sea level pressure), and area-average relative vorticity (1000–850-mb layer) are compared. These terms provide general descriptions of the strength of the low-level cyclogenesis in the two groups and indicate our success in forming these groups from the SLP charts. Next, two low tropospheric diagnostic terms, the area-average vertical static stability (1000–500 mb, 1000–800 mb) and the low-level baroclinicity (1000–500- and 1000–800-mb layers) are described. Finally, three related upper tropospheric terms, the area-average kinematic vertical velocity (700-mb level), outward mass flux (500–200 mb), and area-average absolute vorticity advection (500–200 mb) are presented. These terms are chosen because they can be easily evaluated using the budget volume approach. They are used to test the approach of this paper, forming composites of the diagnostic terms rather than diagnostics of the composite fields.

The kinematic vertical velocity is obtained from the vertically integrated continuity equation in pressure coordinates. The vertical mass flux is computed at each level by determining the mass divergence from the surface to 10 mb (utilizing ECMWF vertical motion values for the top and bottom boundary values). Since the lateral flux of mass is calculated from the wind fields, errors in balancing the vertical and horizontal divergence occur that produce a computed top vertical mass flux that does not equal the observed ECMWF value. The O'Brien (1970) correction scheme is utilized to distribute this residual error over all the pressure layers. The weighting of this adjustment is increased linearly with height since the winds are more difficult to measure at higher heights.

Several methods to measure the strength of the low-level baroclinicity were considered using vertically averaged temperature differences at the storm boundary on a diameter through the storm center. The following different diameters were considered when evaluating this term:

- a diameter perpendicular to storm motion,
- a diameter through the storm center from the warmest area in the warm sector, and
- a diameter through the storm center to the coldest point north to northwest of the cyclone.

The maximum temperature difference from either the warmest or coldest points along a diameter through the storm center was chosen as the best technique due to its better representation of the thermal wind and reproducibility. The maximum value of these temperature differences was chosen as a measure of the strength of the low-level frontal zone or baroclinity.

The static stabilities were derived from the ECMWF temperature analyses. Only dry stability measure was computed because of concern for the quality of the moisture analyses over the ocean. Moist measures of stability should be added to the diagnostics in the future.

Results of the computations of these cyclone development parameters are included in the next section. The results for the initial time highlight the major differences in the storm environment properties between the explosive and nonexplosive groups. Diagnostic results for the 12- and 24-h marks document the amount of cyclogenesis for the two collections of storms.

5. Results

Differences between rapid and nonrapid cyclogenesis are evaluated by comparing diagnostic terms for the two groups of cyclones. These terms are compared after the start of deepening at the different time intervals (0, 12, and 24 h) for the 24-h cyclogenesis period. The evaluation of these parameters is performed in a storm-centered framework using averages from 4° and 6° latitude radii budget volumes. Hereafter, these volumes will be referred to as 4°/6° volumes.

Statistical box plots provide a convenient method to display data distributions by using quartiles (Chambers et al. 1983; Turkey 1977). The 12-h change in pressure ΔP in Fig. 3 illustrates this type of display. The first two plots (going left to right) are the initial 12-h changes in pressure for the explosive (EX) and nonexplosive (NEX) storm groups. The two plots on the right are for the next 12-h development period. The medians (horizontal line segment within the box) for the initial 12-h period are 12 mb for the explosive cyclones and 6 mb for the nonexplosive ones. The circles within the boxes represent the means (13 mb) for explosive and (6 mb) for nonexplosive cyclones. Means and standard deviations are given by Table 1. The top

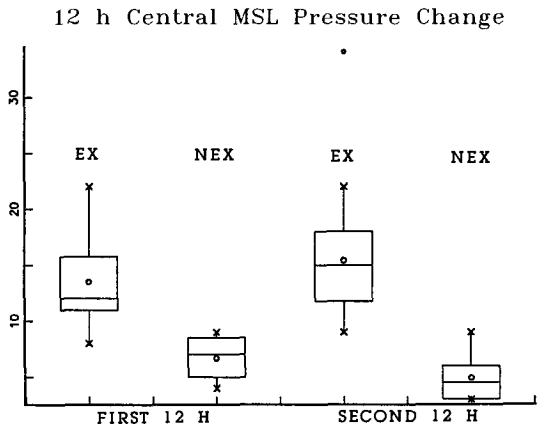

FIG. 3. Box plots of 12-h pressure changes (mb) of the rapid and nonrapid deepening groups of cyclones for the first and second 12-h development periods. Additional explanation of the box plots is given in the text.

TABLE 1. Mean 12-h MSL pressure decrease for explosive and nonexplosive storms. Standard deviations are listed in parentheses.

MSL central pressure change (mb)	Explosive	Nonexplosive
0–12 h	13.52 (3.55)	6.67 (1.72)
12–24 h	15.41 (6.13)	4.93 (1.94)

of the box for the explosive storms at the first 12-h period represents the 75th percentile (16 mb) and the bottom is the 25th percentile (11 mb) for the 23 storms in this group. The interquartile range Q is the distance from the bottom of the box to the top (Chambers et al. 1983). The value of Q is used to define the following terms:

- adjacent values indicated by x are within $1.5Q$ of the quartiles,
- outside points indicated by nonconnected smaller circles are between $1.5Q$ and $3Q$ of the quartiles, and
- detached points indicated by a solid circle are greater than $3Q$ away from the quartiles.

The clear separation of the explosive and nonexplosive 12-h pressure changes in the box plots reflects the rapid development definition of the two cyclone groups from the MSL pressure maps. The rapid cyclogenesis criterion is approximately 9 mb (12 h)$^{-1}$ for the 40°–50°N latitude range of these storms.

The box plots allow a partial assessment of symmetry. If the distribution is symmetric, then the box plot is symmetric about the median. Additionally, if the distance to the upper adjacent point from the top of the box is greater than the lower distance from the bottom, then the data distribution is skewed to the higher pressure change as in the case of the explosive storms (for the first 12-h interval in Fig. 3). The explosive storms have a higher mean (represented by a circle) and median than the nonexplosive ones, following the definition of the groups. The variability of the data for the explosive storms is greater during both time periods, as shown in Fig. 3 and Table 1. This graphic representation provides a method to compare average values and also the distribution of different diagnostic terms.

The Mann–Whitney (M–W) two-sample rank test is used to test the significance of the difference of the means of each of the populations (explosive vs nonexplosive parameters). The null hypothesis that the populations are equal is rejected at a 0.10 significance level if the Mann–Whitney statistic gives a critical level (P value) less than 0.10. Terms that are found by the M–W test to have separable means have their P values annotated in Tables 2–7 with "**."

The M–W test is not as powerful when working with normal data as the more familiar t test (Conover 1980). However, it is used because it does not require normally distributed data. Testing for a normal distribution has questionable significance for small samples.

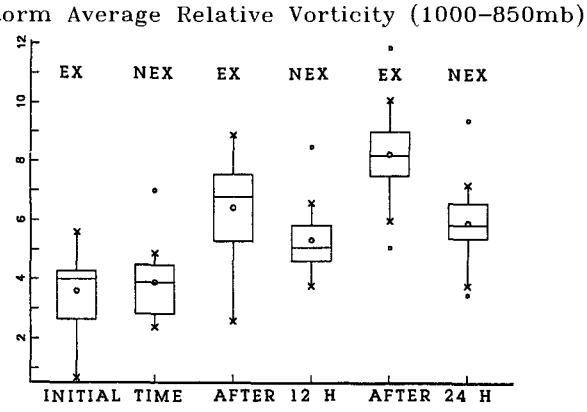

FIG. 4. Box plots of 4° budget volume average relative vorticity (10^{-5} s^{-1}) for the 1000–850-mb layer for the initial time, 12, and 24 h later.

a. Time tendency of low-level circulation

The strength of the low-level circulation is measured by the storm average relative vorticity for the 1000–850-mb layer (Fig. 4). The values at the start of cyclogenesis (Table 2) show no overall difference (explosive storms slightly weaker than nonexplosive storms for both volumes). The differences are far from significant and largely reflect the variability in defining and capturing the initial growth period when 12-h time resolution is used. The fact that the initial values are nearly identical for the explosive and nonexplosive cases indicate that the 0-h low-level intensity is comparable between the two groups.

Gyakum (1991) recently reported positive correlations of early development before the explosive deepening (antecedent deepening) with subsequent explosive deepening. Our results differ with Gyakum in that the explosive and nonexplosive cases are of similar strength at 0 h. We did not compute a 12-h antecedent

TABLE 2. 24-h evolution of storm average low-level (1000–850 mb) relative vorticity (10^{-5} s^{-1}) (4° and 6° radii). Standard deviations are listed in parentheses. The P values for the separation of explosive and nonexplosive storms at the 90% level of confidence are indicated by **.

	Explosive (10^{-5} s^{-1})	Nonexplosive (10^{-5} s^{-1})	P value
		4°	
0 h	3.61 (1.26)	3.91 (1.20)	0.66
12 h	6.44 (1.62)	5.40 (1.20)	0.03**
24 h	8.26 (1.63)	5.93 (1.46)	0.002**
		6°	
0 h	2.08 (0.88)	2.14 (0.92)	0.94
12 h	3.54 (0.97)	2.71 (0.805)	0.01**
24 h	4.10 (0.96)	3.08 (0.983)	0.01**

deepening statistic for those cases where a previous cyclone can be found. This would allow a better comparison with Gyakum's results.

As the storm development progresses, the explosive cyclones exhibit much larger relative vorticity increases over the 24-h development period, both at 4° and 6° volumes. The 4° average vorticity of the explosive group nearly triples in 24 h. Both the 12- and 24-h values of the explosive and nonexplosive cases of relative vorticity are statistically separable at the 99% confidence level (Table 2). For the 6° radius the increase in relative vorticity during the 24-h development is less dramatic than for the 4° radius. The differences, though, are still significant after 12 and 24 h. These differences indicate that we were successful in selecting the explosive and nonexplosive groups from the SLP analyses and that the ECMWF analyses clearly resolve the rapid low-level vorticity buildup associated with the central pressure falls of these oceanic deepening storms.

b. *Time tendency of static stability*

To explore the thermodynamic and dynamic factors responsible for the different rates of development, a number of terms are evaluated. First, the storm average static stability in the 1000–500-mb layer (Fig. 5 and Table 3) is evaluated. The results show that both explosive and nonexplosive systems develop in a weak static stability environment. The dry static stability values ($\partial\theta/\partial p$) for the explosive storms are approximately 0.7 K (100 mb)$^{-1}$ less than the nonexplosive storms initially. This agrees with the expected reduced static stability for the more rapid deepening storms. However, Fig. 5 shows considerable overlap of the explosive and nonexplosive storm distributions. The initial dry static stability analyses, like the initial low-level vorticity, cannot be used to separate the nonexplosive from explosive cyclone groups. However, the standard deviation is larger for nonexplosive storms for the initial

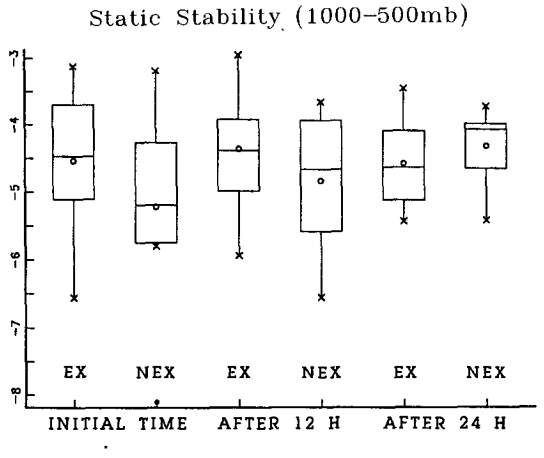

FIG. 5. As in Fig. 4 except for static stability as measured by $\partial\theta/\partial p$ [K (100 mb)$^{-1}$].

TABLE 3. 24-h evolution of static stability for both storm groups (4° and 6° radii). Standard deviations are listed in parentheses.

1000–500 mb ($\partial\theta/\partial p$)	Explosive [K (100 mb)$^{-1}$]	Nonexplosive [K (100 mb)$^{-1}$]	P value
	4°		
0 h	−4.53 (1.01)	−5.21 (1.56)	0.253
12 h	−4.36 (0.81)	−4.84 (1.05)	0.485
24 h	−4.57 (0.65)	−4.32 (0.62)	0.482
	6°		
0 h	−4.68 (0.93)	−5.04 (1.07)	0.27
12 h	−4.50 (0.71)	−4.86 (0.89)	0.26
24 h	−4.63 (0.59)	−4.59 (0.61)	0.80

and 12-h time. This suggests that higher static stability is a factor in the weak development of some of these cases.

Although the average static stability is similar for the explosive and nonexplosive cyclones, there still may be particular quadrants or regions of the cyclone for which there are large static stability differences. Quadrants about the storm center were defined by the storm motion vector at a given time period. An analysis of the static stability for the four quadrants of the storm volume indicates that the explosive storms in the left front quadrant are up to 0.8° K (100 mb)$^{-1}$ less stable, a result similar to the entire cyclone stability results. This difference is not significant at the 0- or 12-h mark. The lack of significant differences during development implies only an inconclusive role of static stability on the degree of development. It should be repeated that the role of vertical moisture variations is not included in this term. A moist static stability measure should be studied given confidence in the moisture analysis, and such a statistic may show more differences between the two groups.

c. *Time tendency of low-level baroclinity*

The strength of the low-level baroclinic structure is estimated from the 1000–500-mb layer average temperature differences across the storm budget volume, as shown in Fig. 6 and Table 4. The nonexplosive storm's baroclinicity as measured by this temperature difference is actually slightly larger than the explosive storm's, particularly at the 12- and 24-h marks. However, wide variability for both explosive and nonexplosive storms limits statistical significance. The similarity of the frontal zone strength between the two groups is interesting. The theoretical and modeling results of James (1987) and others have suggested the deformation associated with strong horizontal shears may significantly reduce growth rates associated with baroclinic instabilities. This effect may account for the relative lack of correlation between deepening rates and baroclinity.

The frontal zone strength weakens during the 24-h development period, particularly for the explosive

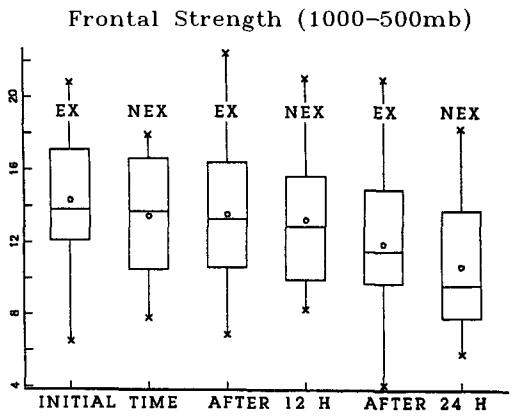

FIG. 6. As in Fig. 4 except for large-scale baroclinity as measured by maximum temperature difference (K) across the cyclone.

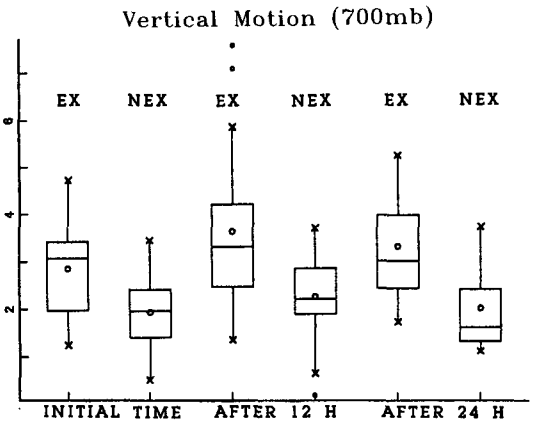

FIG. 7. As in Fig. 4 except for 700-mb kinematic vertical motion ($\mu b\ s^{-1}$).

storm group. For nonexplosive storms there is a tendency to strengthen for the first 12 h. That the nonexplosive storms retain a high degree of baroclinicity simply reflects their lack of development and associated weaker conversion of available potential to kinetic energy.

d. Time tendency of vertical motion

The sample statistics for the 700-mb kinematic vertical velocities (units of 10^{-3} mb s^{-1}) at 4° and 6° volumes are shown in Fig. 7 and Table 5. The key result is a clear separation of average vertical motion for both the 4° and 6° volumes of the explosive and nonexplosive groups at the initial time. Significant upward vertical motion exists in the early stages of storm development for explosive storms.

It is not surprising to find stronger vertical motion values for the explosive group during rest of the time periods at both the 4° and 6° radii. These large vertical motion values are consistent with the subsequent strong low-level vorticity increases and pressure falls, and occur in part due to intensified diabatic processes associated with the rapid deepeners. The maximum vertical velocity generally occurs 12 h into the deepening.

e. Time tendency of upper-level divergence and vorticity advection

We turn to the upper-level outward mass flux (divergence) and vorticity advection to explore further differences in the upper troposphere for the initial time of development. The strength of these upper-level terms is estimated from the 300-mb layer that contained the strongest outward mass flux and absolute vorticity advection (both storm and earth relative). Typically, this layer is bounded by the 500- and 200-mb surfaces. Major differences between rapid and normal cyclogenesis at the initial period are also found in these terms. The upper-level outward mass transport (Fig. 8 and Table 6) indicates stronger divergence at the initial time for the explosive cases. Figure 9 and Table 7 show that the storm average vorticity advection is significantly larger for the explosive cases at the 0-h mark. These two terms plus the vertical motion results confirm significant differences in the upper troposphere between the two groups when surface systems are weak and of equal strength. This result supports the synoptic observations of Sanders (1986) of 500-mb upper-level disturbances present before rapid development.

TABLE 4. 24-h evolution of thermal strength for both storm groups (4° and 6° radii). Standard deviations are listed in parentheses.

1000–500 mb	Explosive (K)	Nonexplosive (K)	*P* value
	4°		
0 h	14.30 (3.42)	13.46 (3.53)	0.49
12 h	13.56 (3.77)	13.25 (3.88)	0.80
24 h	11.90 (4.64)	10.64 (3.56)	0.25
	6°		
0 h	19.44 (4.51)	18.19 (4.64)	0.30
12 h	18.10 (4.63)	17.52 (5.06)	0.59
24 h	16.29 (5.11)	14.78 (3.90)	0.17

TABLE 5. 24-h evolution of 700-mb kinematic vertical motion (4° and 6° radii). Standard deviations are listed in parentheses. The *P* values for the separation of explosive and nonexplosive storms at the 10% level of confidence are indicated by **.

700-mb omega	Explosive (10^{-3} mb s^{-1})	Nonexplosive (10^{-3} mb s^{-1})	*P* value
	4°		
0 h	−2.86 (0.97)	−1.93 (0.84)	0.010**
12 h	−3.65 (1.63)	−2.26 (0.97)	0.010**
24 h	−3.33 (1.14)	−1.99 (0.93)	0.007**
	6°		
0 h	−2.07 (0.61)	−1.65 (0.85)	0.13
12 h	−2.74 (0.99)	−1.82 (0.76)	0.01**
24 h	−2.55 (0.91)	−1.51 (0.67)	0.01**

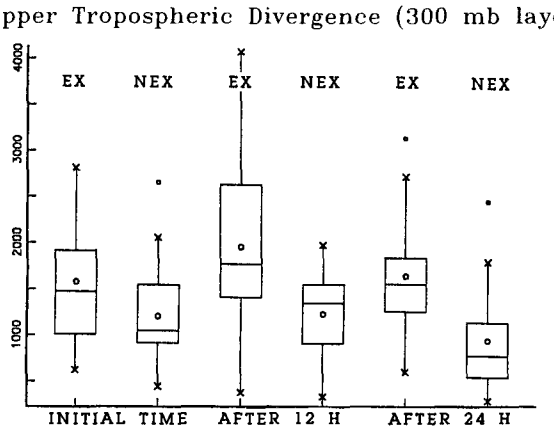

FIG. 8. As in Fig. 4 except for upper-level divergence, as estimated by maximum outward mass transport (10^{10} g s^{-1}) in a upper-tropospheric layer. Evaluated for a layer 300 mb thick.

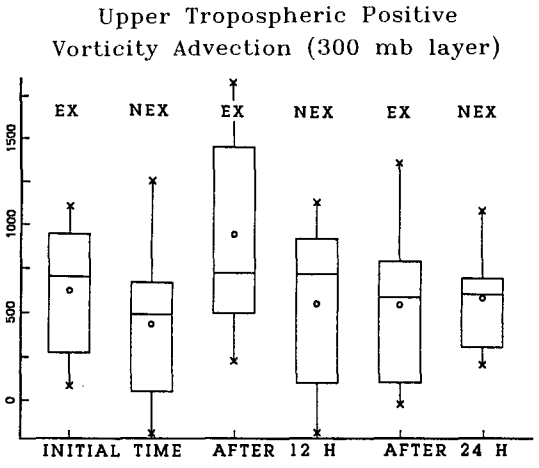

FIG. 9. As in Fig. 8 except for positive absolute vorticity advection (10^{-11} s^{-2}) for 300-mb layer.

The results from 12- and 24-h marks confirm the strong differences in the subsequent development. The initially strong positive vorticity advection becomes more intense during the first 12 h, presumably through the self-development process (Petterssen 1956). In the explosive cases, the vorticity advection is double the nonexplosive magnitude at the 12-h mark for the 4° radius. At the 24-h mark, the explosive group still has stronger advection, but unlike the previous time periods, it is no longer statistically significant at the 4° radius. The results of the two groups at 12 and 24 h provide confidence in the analyses from which the diagnostics are based. Both the low-level vorticity and thermal strength, and the upper-level vertical motion, outward mass flux, and vorticity advection document the more intense development of the explosive group in agreement with classical cyclogenesis theory.

6. Summary and conclusions

During the past decade there has been considerable interest in characteristics of explosive storms. Less attention has been paid to weaker cyclones and comparisons between the development of intense versus ordinary systems. In this paper diagnostic terms for both explosive and nonexplosive cyclones have been contrasted for their initial development period. Cyclones that occurred during the FGGE SOP 1 winter were investigated using the revised ECMWF analyses. To compute statistics for similar regions of all the storms, a translating storm environment budget volume was used to evaluate a variety of diagnostic terms found to be important to cyclogenesis.

Major differences between explosive and nonexplosive systems were found at the start of deepening in the strength of the upper-level processes and their coupling to the developing cyclone. Explosive systems had stronger upper-level divergence and stronger positive vorticity advection at this initial development time. In addition, the explosive systems had more vigorous upward vertical motion, indicating the coupling of the upper-level divergence with the incipient surface system. This dataset indicates that the presence of an upper-tropospheric wave and the associated upper-level divergence area are indicators of subsequent rapid development in agreement with Sanders (1986) and Manobianco (1989).

TABLE 6. 24-h evolution of upper-level mass divergence averaged for 300-mb layer (4° and 6° radii). Standard deviations are listed in parentheses and ** indicates explosive and nonexplosive sets are statistically different at a 90% confidence level.

	Explosive (10^{10} g s^{-1})	Nonexplosive (10^{10} g s^{-1})	P value
	4°		
0 h	1581 (614)	1208 (602)	0.07**
12 h	1956 (892)	1230 (485)	0.01**
24 h	1643 (646)	947 (601)	0.004**
	6°		
0 h	2569 (959)	2348 (1218)	0.33
12 h	3304 (1318)	2213 (1023)	0.01**
24 h	2936 (1203)	1661 (1022)	0.005**

TABLE 7. 24-h evolution of upper-level positive vorticity advection averaged for 300-mb layer (4° and 6° radii). Standard deviations are listed in parentheses and ** indicates explosive and nonexplosive sets are statistically different at a 10% confidence level.

	Explosive (10^{-11} s^{-2})	Nonexplosive (10^{-11} s^{-2})	P value
	4°		
0 h	1057 (720)	647 (528)	0.06**
12 h	1499 (894)	705 (579)	0.01**
24 h	1051 (645)	751 (333)	0.17
	6°		
0 h	673 (323)	504 (363)	0.20
12 h	963 (563)	684 (370)	0.16
24 h	784 (355)	541 (278)	0.07**

The initial low-level vorticity, frontal strength, and static stability were not significantly different between the two groups. Comparisons of the dry vertical static stability showed the rapid developers to be somewhat more unstable. However, the two groups are not statistically different. Static stability of quadrants of the storm were evaluated, with the smallest static stability found in the forward left quadrant. However, a moist static stability measure was not computed in this study.

The strength of the frontal zone for these cyclones was evaluated by computing the temperature gradient across the frontal zone. The explosive systems did not have a stronger baroclinic zone. In fact, the nonexplosive systems had somewhat larger frontal-zone temperature differences.

This study of composites of the diagnostics of 38 storms indicates that the lower-tropospheric environment of the explosive and nonexplosive cyclones appear to be similar. Dry static stability is weak, particularly in the front left quadrant, and the systems develop on a strong frontal zone. Both the explosive and nonexplosive groups of cyclones had similar central pressures and low-level vorticity values, so the explosive systems were not stronger at the initial time. An interesting difference between the two groups at 0 h is the presence of a more organized upper-level system with significant upper-level divergence and upward vertical motion. The presence of an upper-level source of divergence properly phased with the low-level incipient system is crucial for the subsequent rapid development for this dataset. These results support the conclusions of Sanders (1986) and Manobianco (1989) that explosive cyclogenesis is a baroclinic phenomenon in which strong upper-tropospheric forcing is enhanced by a weakly stratified marine atmosphere. The 12- and 24-h diagnostics confirm that the ECMWF analyses capture significant differences in the upper- and lower-level measures of development for these oceanic cases and give additional confidence to the results.

The number of cyclones in the explosive and nonexplosive groups is limited. In addition, other aspects of cyclones such as the presence of symmetric instability, the magnitude of upper-tropospheric potential vorticity anomalies, and the role of diabatic processes need to be explored with these collections of explosive and nonexplosive cyclones. Additional research should explore the use of composite diagnostics to study differences between rapid and nonrapid development.

Acknowledgments. Thanks are due to Professor Russell Elsberry, who provided helpful advice on the conduct of the research, and Dr. Paul Hirschberg and the anonymous reviewers who provided helpful comments on the manuscript. Ms. Penny Jones skillfully aided in typing the manuscript. This research was supported in part by National Aeronautics and Space Administration Global Scale Atmospheric Processes Research program under Contract 623-GW-86B. The computations were done at the Church Computer Center of the Naval Postgraduate School.

APPENDIX

Explosive and Nonexplosive Cyclones in the North Pacific and Atlantic Oceans

TABLE A1. Explosive cyclone positions in the North Pacific and Atlantic oceans, from ECMWF analyses, 1979. The asterisk (*) denotes storms with 12-h deepening. Time is in UTC.

	Start time	0 h	12 h	24 h
Pacific Ocean				
P1	18 January/0000	40.2°N,139.1°E	39.5°N,147.7°E	42.2°N,157.2°E
P2	26 January/0000	33.7°N,145.0°E	34.5°N,154.0°E	35.2°N,162.8°E
P3	5 February/1200	31.5°N,134.0°E	36.0°N,141.0°E	42.0°N,146.0°E
P4*	10 February/1200	49.0°N,164.0°E	51.3°N,168.0°E	55.2°N,169.0°E
P5	15 February/1200	37.5°N,141.5°E	39.3°N,149.0°E	43.0°N,158.0°E
P6	17 February/1200	37.0°N,145.5°E	42.7°N,153.5°E	48.5°N,156.2°E
P7	25 January/1200	40.3°N,178.5°E	45.4°N,177.5°W	48.7°N,179.9°E
P8*	28 January/0000	37.3°N,161.0°E	40.0°N,168.0°E	42.0°N,170.0°E
P9*	19 February/0000	42.8°N,146.3°E	40.8°N,153.5°E	42.2°N,161.7°E
P10	4 March/0000	30.0°N,142.0°E	32.2°N,148.0°E	33.8°N,152.8°E
P11	3 January/0000	35.4°N,170.7°E	38.6°N,176.0°W	41.2°N,168.0°W
P12	10 January/0000	40.5°N,133.8°E	44.3°N,149.9°E	47.5°N,161.5°E
P13	12 January/1200	32.1°N,142.0°E	33.9°N,151.0°E	36.9°N,161.8°E
P14*	31 January/0000	38.3°N,171.5°W	43.2°N,168.4°W	48.8°N,168.5°W
Atlantic Ocean				
A1	18 January/1200	41.5°N,63.5°W	40.5°N,58.5°W	43.3°N,52.5°W
A2	28 January/1200	36.7°N,71.5°W	39.3°N,62.0°W	42.0°N,58.6°W
A3	31 January/1200	33.5°N,78.0°W	35.0°N,70.5°W	37.2°N,62.0°W
A4	10 February/0000	33.3°N,69.3°W	37.6°N,55.2°W	42.0°N,41.7°W
A5	13 February/1200	36.2°N,66.6°W	39.0°N,54.2°W	47.7°N,42.8°W
A6	19 February/0000	31.5°N,77.0°W	36.0°N,73.0°W	37.5°N,65.5°W
A7*	15 February/1200	47.0°N,39.0°W	54.8°N,32.6°W	61.2°N,34.8°W
A8	2 January/1200	46.9°N,40.0°W	47.7°N,32.0°W	48.4°N,26.2°W
A9*	20 February/0000	49.5°N,24.2°W	57.3°N,19.0°W	59.7°N,21.5°W

TABLE A1. Explosive cyclone positions in the North Pacific and Atlantic oceans, from ECMWF analyses, 1979. The asterisk (*) denotes storms with 12-h deepening. Time is in UTC.

	Start time	0 h	12 h	24 h
Pacific Ocean				
NP1	21 January/1200	39.0°N,148.0°E	41.0°N,158.5°E	43.0°N,168.0°E
NP2	31 January/1200	37.2°N,133.5°E	40.5°N,136.7°E	43.3°N,140.0°E
NP3	4 February/0000	43.6°N,144.0°E	46.0°N,150.0°E	50.8°N,153.0°E
NP4	21 February/0000	51.5°N,142.0°E	52.0°N,148.0°E	53.5°N,151.0°E
NP5	13 February/1200	40.3°N,132.0°E	42.0°N,138.3°E	46.2°N,143.0°E
NP6	26 February/1200	33.9°N,142.5°E	35.3°N,147.0°E	37.3°N,151.3°E
NP7	1 January/0000	38.5°N,168.0°W	41.3°N,157.7°W	43.0°N,155.0°W
NP8	5 January/1200	31.5°N,159.8°E	34.8°N,167.0°E	35.8°N,175.5°E
NP9	16 January/1200	43.0°N,178.0°W	47.6°N,166.6°W	51.9°N,156.6°W
NP10	14 January/1200	42.2°N,163.0°E	44.0°N,174.5°E	46.7°N,173.5°W
NP11	23 January/0000	45.0°N,176.5°E	48.6°N,175.0°W	51.7°N,169.6°W
NP12	24 February/0000	35.1°N,145.1°E	36.3°N,148.2°E	36.8°N,150.8°E
Atlantic Ocean				
NA1	7 February/1200	34.0°N,78.0°W	37.5°N,71.5°W	41.0°N,64.0°W
NA2	22 February/1200	45.5°N,65.0°W	44.0°N,56.0°W	39.0°N,48.0°W
NA3	11 January/0000	41.6°N,48.6°W	48.0°N,40.0°W	50.9°N,32.0°W

TABLE A3. MSL central pressure for explosive cyclones in the North Pacific and Atlantic oceans, from ECMWF analyses, 1979. The asterisk (*) denotes storms with 12 h of deepening. Time is in UTC.

	Start time	0 h	12 h	24 h
Pacific Ocean				
P1	18 January/0000	1006	984	968
P2	25 January/0000	1006	994	985
P3	5 February/1200	1015	1003	988
P4*	10 February/0000	1003	992	985
P5	17 February/1200	999	983	974
P6	15 February/1200	997	989	977
P7	25 January/1200	991	977	968
P8*	28 January/0000	996	980	978
P9*	19 February/0000	999	989	984
P10	4 March/0000	1008	995	977
P11	3 January/0000	1004	991	976
P12	10 January/0000	1014	993	971
P13	12 January/1200	1007	995	984
P14*	31 January/0000	1007	991	986
Atlantic Ocean				
A1	18 January/1200	1002	987	975
A2	28 January/1200	991	976	960
A3	31 January/1200	1010	999	979
A4	10 February/0000	1006	995	961
A5	13 February/1200	1004	992	979
A6	19 February/0000	1020	1010	992
A7*	15 February/1200	986	967	967
A8	2 January/1200	1009	998	985
A9*	20 February/0000	992	981	984

TABLE A4. MSL central pressure for nonexplosive cyclone in the North Pacific and Atlantic oceans, from ECMWF analyses, 1979. Time is in UTC.

	Start time	0 h	12 h	24 h
Pacific Ocean				
NP1	21 January/1200	1004	999	996
NP2	31 January/1200	1007	998	996
NP3	4 February/0000	1014	1007	1004
NP4	21 February/0000	996	987	983
NP5	13 February/1200	1011	1005	996
NP6	26 February/1200	1002	995	988
NP7	1 January/0000	1001	996	990
NP8	5 January/1200	1005	1000	994
NP9	16 January/1200	999	990	984
NP10	14 January/1200	993	986	979
NP11	23 January/0000	999	990	985
NP12	24 February/0000	993	986	983
Atlantic Ocean				
NA1	7 February/1200	1005	1000	996
NA2	22 February/1200	1005	1000	997
NA3	11 January/0000	1012	1006	1003

REFERENCES

Bengtssen, L., M. Kanamitsu, P. Kallberg, and S. Uppala, 1982: FGGE 4-dimensional data assimilation at ECMWF. *Bull. Amer. Meteor. Soc.*, **63,** 29–43.

Chambers, J. M., W. S. Cleveland, B. Kleiner, and P. A. Tukey, 1983: *Graphical Methods for Data Analysis.* Duxbury Press, 395 pp.

Conover, W. J., 1980: *Practical Nonparametric Statistics.* 2d ed. Wiley & Sons, 462 pp.

Gyakum, J. R., 1991: Life cycles of surface cyclones in the western North Pacific. Preprints, *the First International Symp. on Winter Storms,* New Orleans, Amer. Meteor. Soc., 40–43.

——, J. Anderson, R. Grumm, and E. Gruber, 1989: North Pacific cold-season surface cyclone activity: 1975–1983. *Mon. Wea. Rev.*, **117,** 1141–1155.

Halem, M., E. Kalnay, W. E. Baker, and R. Atlas, 1982: An assessment of the FGGE satellite observing system during SOP-I. *Bull. Amer. Meteor. Soc.*, **63,** 407–427.

James, I. N., 1987: Suppression of baroclinic instability in horizontal sheared flows. *J. Atmos. Sci.*, **44,** 3710–3720.

Johnson, D. R., and W. K. Downey, 1975a: Azimuthally averaged transport and budget equations for storms: Quasi-Lagrangian diagnostics. *Mon. Wea. Rev.*, **103,** 967–979.

——, and W. K. Downey, 1975b: The absolute angular momentum of storms: Quasi-Lagrangian diagnostics. *Mon. Wea. Rev.*, **103,** 1063–1076.

Kuo, Y.-H., and S. Low-Nam, 1989: Prediction of nine explosive cyclones over the western Atlantic Ocean with a regional model. *Mon. Wea. Rev.*, **118,** 3–25.

Manobianco, J., 1989: Explosive east coast cyclogenesis over the west-central North Atlantic Ocean: A composite study derived from ECMWF operational analyses. *Mon. Wea. Rev.*, **117,** 2365–2383.

Mullen, S. L., and D. P. Baumhefner, 1988: Sensitivity of numerical simulations of explosive oceanic cyclogenesis to changes in physical parameterizations. *Mon. Wea. Rev.*, **116,** 2289–2329.

O'Brien, J. J., 1970: Alternative solutions to the classical vertical velocity problem. *J. Appl. Meteor.*, **2,** 197–203.

Paegle, J., 1986: Summary of the national conference on the scientific results of the First GARP Global Experiment, 14–17 January, 1986. *Bull. Amer. Meteor. Soc.*, **67,** 1487–1492.

Petterssen, S., 1956: *Weather Analysis and Forecasting.* Vol. 1. *Motion and Motion Systems.* McGraw-Hill, 428 pp.

Roebber, P. J., 1984: Statistical analysis and updated climatology of explosive cyclones. *Mon. Wea. Rev.*, **112,** 1577–1589.

Rogers, E., and L. F. Bosart, 1986: An investigation of explosive deepening oceanic cyclones. *Mon. Wea. Rev.*, **114,** 702–718.

Sanders, F., 1986: Explosive cyclogenesis in the west-central North Atlantic Ocean 1981–84. Part I: Composite structure and mean behavior. *Mon. Wea. Rev.*, **104,** 1781–1794.

——, and J. R. Gyakum, 1980: Synoptic-dynamic climatology of the "bomb". *Mon. Wea. Rev.*, **108,** 1589–1606.

Shaw, D. B., P. Lonnberg, A. Hollingsworth, and P. Unden, 1987: Data assimilation: The 1984/85 revisions of the ECMWF mass and wind analysis. *Quart. J. Roy. Meteor. Soc.*, **113,** 533–566.

Smith, D. H., 1986: A diagnostic investigation of explosive maritime cyclogenesis during FGGE. M.S. thesis, Naval Postgraduate School, Monterey, CA, 53 pp.

Turkey, J. W., 1977: *Exploratory Data Analysis.* Addison-Welsley Publishing Company, 257 pp.

Uppala, S., 1986: The assimilation of the final FGGE dataset at ECMWF. Part I. *Proc. of the U.S. National Conference on the Scientific Results of the First GARP Global Experiment.* Amer. Meteor. Soc., Miami, 24–30.

Wash, C. H., J. E. Peak, W. E. Calland, and W. A. Cook, 1988: Diagnostic study of explosive cyclogenesis during FGGE. *Mon. Wea. Rev.*, **116,** 431–451.